

Graphene–Silica Composite Thin Films as Transparent Conductors

Supinda Watcharotone,[†] Dmitriy A. Dikin,[†] Sasha Stankovich,[†] Richard Piner,[†] Inhwa Jung,[†] Geoffrey H. B. Dommett,[†] Guennadi Evmenenko,[‡] Shang-En Wu,^{||} Shu-Fang Chen,^{||} Chuan-Pu Liu,^{||} SonBinh T. Nguyen,[§] and Rodney S. Ruoff^{*,†}

Department of Mechanical Engineering, Northwestern University, Evanston, Illinois 60208, Department of Physics and Astronomy, Northwestern University, Evanston, Illinois 60208, Department of Chemistry, Northwestern University, Evanston, Illinois 60208, and Department of Materials Science and Engineering, National Cheng Kung University, Tainan 701, Taiwan

Received February 28, 2007; Revised Manuscript Received April 30, 2007

ABSTRACT

Transparent and electrically conductive composite silica films were fabricated on glass and hydrophilic SiO₂/silicon substrates by incorporation of individual graphene oxide sheets into silica sols followed by spin-coating, chemical reduction, and thermal curing. The resulting films were characterized by SEM, AFM, TEM, low-angle X-ray reflectivity, XPS, UV–vis spectroscopy, and electrical conductivity measurements. The electrical conductivity of the films compared favorably to those of composite thin films of carbon nanotubes in silica.

Electrically conductive glass is used in a broad range of applications such as in solar reflecting windshields,¹ self-cleaning windows,² electrostatic charge-dissipating coatings,^{3,4} solar cells,^{5,6} and sensor devices.^{7,8} Typically, to render it conductive, a substrate is coated with carbon or metal oxide films such as indium tin oxide (ITO) or aluminum-doped zinc oxide (AZO).^{2,7,9–24} However, the conventional fabrication processes for coating these carbon or metal oxide films such as magnetron sputtering deposition,^{11–18} cathodic arc plasma deposition,^{19,20} chemical vapor deposition,^{21,22} or spray pyrolysis²³ are expensive and complex. In addition, although carbon films possess high hardness, conductive carbon coatings do not provide sufficient optical transparency and often have poor adhesion to substrates.¹⁸ Either additional metal interlayers,¹⁸ periodic multilayers of carbon,^{18,19} or pretreatment of substrates with ion implantation^{20,24} is required to promote adhesion of the carbon films to the substrates. Moreover, the metal oxide coatings are susceptible to ion diffusion from the metal oxide films into the substrates, which can be unfavorable for long-term device performance.²⁵ As such, much research has been devoted to find a simple solution-based route to fabricate highly stable electrically conductive thin films.^{7–9,26–32}

Carbon nanotube (CNT) networks are a potential alternative and can be fabricated via a solution-based method. CNTs in an appropriate solvent are filtered using a filter such as porous alumina and transferred to a transparent substrate using polydimethylsiloxane (PDMS) via a printing method.³³ For a large-scale coating process, several sequential transfers of the CNT network are required to cover a large area. Here, we use a simple solution-based method to directly coat an electrically conductive film onto a transparent substrate.

We have been interested in using electrically conductive graphene-based sheets as fillers for a broad range of composite materials. Attempts to exfoliate graphene-based sheets by intercalation of graphite with potassium metal have been discussed,³⁴ however, the exfoliated nanoplatelets are ~10 nm thick, thus having approximately 30 stacked layers. We routinely employed soluble graphene oxide-based sheets^{35,36} produced by complete exfoliation of graphite oxide (GO) as an entry into composites of organic polymers.^{35,37} As these sheets are highly compatible with water, we hypothesized that they would also make an ideal filler for incorporation into inorganic matrices that require aqueous or semi-aqueous processing such as those produced by the sol–gel route via hydrolysis and polycondensation of metal alkoxides. As graphene oxide sheets can be rendered electrically conductive by chemical deoxygenation,^{38,39} their subsequent reduction inside the matrix would lead to electrically conductive inorganic composites. In this report, we utilized this simple strategy to prepare novel transparent and electrically conductive graphene-containing silica films

* Corresponding author. E-mail: r-ruoff@northwestern.edu. Telephone: (847) 467-6596. Fax: (847) 491-3915.

[†] Department of Mechanical Engineering, Northwestern University.

[‡] Department of Physics and Astronomy, Northwestern University.

[§] Department of Chemistry, Northwestern University.

^{||} Department of Materials Science and Engineering, National Cheng Kung University.

on glass. Such graphene–silica composites are chemically inert and perfectly compatible with both glass and hydrophilic SiO₂/silicon substrates. In addition, because their conductivities do not depend on ions, they should not be susceptible to loss of performance due to ion diffusion.²⁵

We employed the well-known hydrolysis of tetramethyl orthosilicate (TMOS)⁴⁰ in the fabrication of the composite films (see Supporting Information). Briefly, GO prepared via the Hummers method⁴¹ was exfoliated in a water/ethanol mixture to produce a stable suspension of individual graphene oxide sheets. Addition of TMOS into this dispersion yielded graphene oxide-containing sols that can be stored at room temperature for several days (weeks for the sols with high weight percentage⁴² of graphene oxide (11 wt %)). Thin composite films can be then prepared from these sols by spin-coating onto hydrophilic substrates of either borosilicate glass or SiO₂/silicon. Solvent evaporation leads to quick gelation, and the resulting composite films were rendered electrically conductive by overnight exposure to an atmosphere that has been saturated with vapor of hydrazine monohydrate, which was shown to chemically reduce graphene oxide sheets into graphene-like sheets.³⁵ Subsequent drying of the samples at 100 °C converts the films into solid matrices after 3 h. Finally, the samples were thermally treated at 400 °C in an inert atmosphere to form consolidated silica films.^{43,44} For details of the sol and thin film preparations, see Supporting Information.

A scanning electron microscopy (SEM) image of a composite film containing 6.6 wt % of graphene oxide after curing (Figure 1a) indicates a homogeneous morphology with a random distribution of dissimilar black and white domains. Parts b and c of Figure 1 contrast high-magnification SEM images of this film before and after high-temperature curing, respectively. In both images, slightly crumpled sheets overlapping each other can be readily observed, indicating a primarily in-plane orientation. Indeed, such planar distribution of the sheets throughout the film thickness is also evident in the transmission electron microscopy (TEM) images of the cross sections of the composite film with 11 wt % of graphene oxide both before (Figure 2b) and after (Figure 2c) curing. The lack of such features in the graphene oxide-free silica film (Figure 2a) suggests that they originate from the embedded sheets. Prior to spin-coating, substrate surfaces were treated with an oxygen plasma in order to increase their hydrophilicity. This step helps improve the adhesion of the sol during spin-coating deposition; it is possible that the consequently larger shear stress is then acting to align the graphene oxide sheets. During the spin-coating process, composite sols experience a combination of in-plane centrifugal and counter-balancing viscous forces on the rotating stage,⁴⁵ and we suggest this leads to stretching and flattening of graphene oxide sheets that might be to some degree crumpled/wrinkled in the colloidal suspension. For example, light-scattering studies of colloidal suspensions of graphite oxide have been analyzed to yield a fractal dimension of 2.54 ± 0.05 (where 2.0 is for a completely flat membrane and 3.0 is highly crumpled and thus compact).⁴⁶ Further study

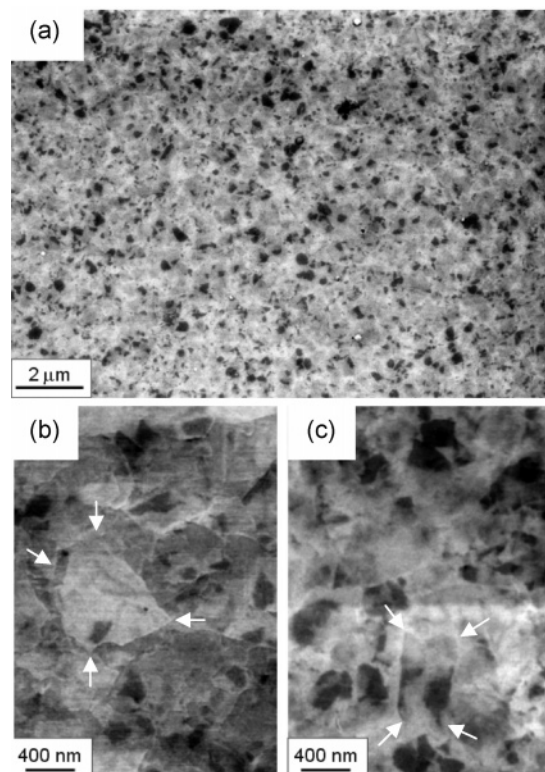


Figure 1. SEM images of 6.6 wt % graphene oxide–silica composite films at: (a) low magnification after high-temperature curing and high magnifications before (b) and after (c) curing. The edges of the sheets were labeled by the white arrows as shown.

of how the sheets end up being so flat in the spun-cast films is indicated.

The thickness of the composite films was determined by both TEM and X-ray reflectivity (XRR) measurements to be ≈ 20 – 30 nm thick. The variation in film thickness determined by XRR fitting for different samples ranged from ± 2 Å to ± 5 Å. Details of XRR data acquisition and analysis procedures are described elsewhere.⁴⁷ Under the conditions employed in this work, the thickness of the films increased slightly with increasing graphene oxide concentration (Figure 2d). In all cases, the thickness of the films decreased after the high-temperature curing step, indicating densification and consolidation of the matrix. We note that, while the film thickness obtained from TEM observation is confined to the cross section of a region smaller than 500 nm across (on a composite sample that is >100 mm² in size), the XRR measurements are more representative of the average thickness, as the X-ray spot size is $\approx 1 \times 20$ mm².

The average surface roughness of the films was quantified by both AFM in contact mode ($\approx 10 \times 10$ μm² area, see Supporting Information) and XRR ($\approx 1 \times 20$ mm² area). The average surface roughness of the films increases with increasing concentration of graphene oxide but decreases after curing. For example, from XRR measurement, the sample with a nominal concentration of 11 wt % graphene oxide had an average surface roughness of ≈ 14 Å before and ≈ 12 Å after curing, while for the 5 wt % sample, the values were ≈ 9 Å and ≈ 8 Å, respectively (Figure 2d). The surface roughness values given from AFM measurements

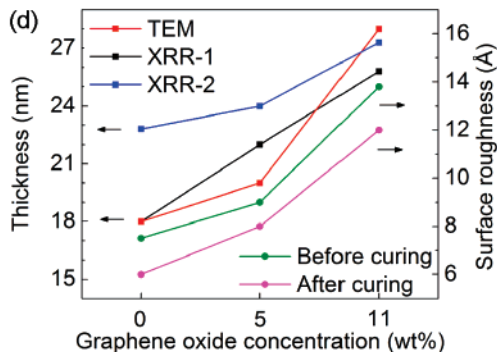
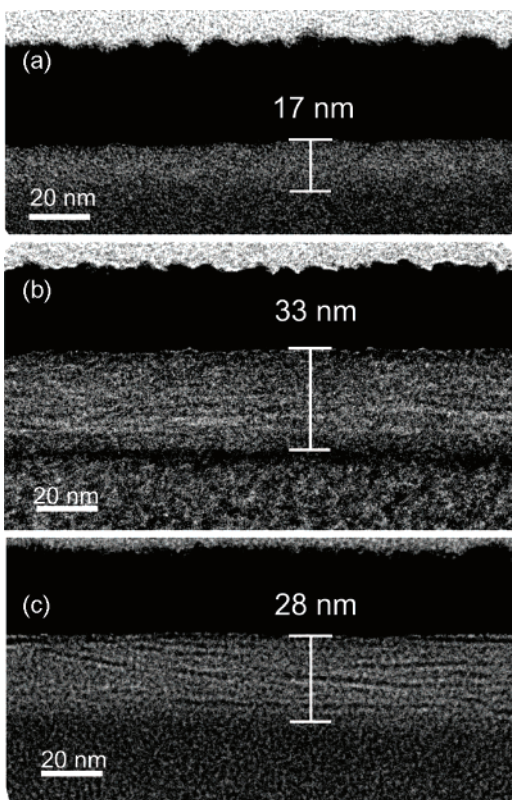


Figure 2. TEM images of the cross sections of the sol-gel derived composite films with (a) 0 wt %, (b) 11 wt % of graphene oxide before the high-temperature curing, and (c) 11 wt % of graphene oxide after the high-temperature curing. The layers are, from the bottom, the glass substrate, composite film, Pt layer, and carbon layer. (d) The plots of the film thickness of the same samples after curing obtained from both TEM and XRR and the surface roughness obtained from XRR before and after curing.

are similar (see Supporting Information). The films are thus relatively smooth and geometrically uniform over both local regions (AFM) and the entire substrate (XRR). XRR data also indicate that the films are reasonably porous (estimated to be from 20 to 40% less dense than the borosilicate glass substrate, depending on humidity level, see Supporting Information), and this density does not change before and after curing. The density of these composite films remains the same (within the limits of measurement uncertainties) over the range of graphene oxide concentrations employed (1–11 vol %).

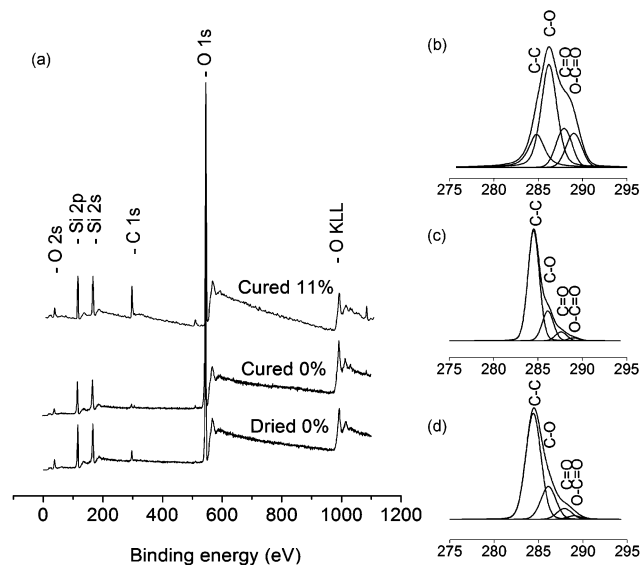


Figure 3. (a) XPS survey spectra of a pure silica (0 wt % graphene oxide) film dried at 100 °C and cured at 400 °C and a composite film containing 11 wt % graphene oxide after being cured at 400 °C. (b–d) C 1s XPS spectra of the 11 wt % composite film (b) after drying, (c) after chemical reduction, and (d) after both chemical reduction and high-temperature curing.

The chemical composition of both the matrix and the filler were monitored by X-ray photoelectron spectroscopy (XPS) during each of the preparation steps. The curing step results in a significant decrease in the carbon content, as seen in the survey XPS spectra of the dried and cured pure silica film (Figure 3a), indicating essentially complete hydrolysis of TMOS. The cured film with 11 wt % graphene oxide exhibited a significantly higher carbon signal compared to that observed for the graphene oxide-free film, indicating the presence of the graphene-based filler (Figure 3a). Specifically, the C 1s XPS spectrum of the composite film with 11 wt % graphene oxide before reduction and curing (Figure 3b) is quite similar to that of graphite oxide itself.³⁵ This region can be deconvoluted into four components corresponding to carbon atoms in different oxygen-containing functional groups:³⁵ (a) the non-oxygenated C at 284.8 eV, (b) the carbon in C–O at 286.2 eV, (c) the carbonyl carbon (C=O, 287.9 eV), and (d) the carboxylate carbon (O–C=O, 289.0 eV). The C 1s XPS spectra of the hydrazine-treated film shows the presence of the same functionalities (cf. Figure 3b,c) but with much smaller contribution of the oxygenated carbons (27.6% vs 81.8%), indicating that deoxygenation has occurred. In addition, we expect a small amount of incorporated nitrogen as a consequence of exposure to hydrazine.³⁵

The highest levels of DC electrical conductivity were measured in the composite films that were both chemically reduced *and* thermally cured, with the magnitude of electrical conductivity increasing with the loading of the graphene oxide. The lowest measured conductivity (resistance < 1 GΩ for our equipment) could be observed at loadings as low as 3.9 wt % of graphene oxide. As a control, pure silica films that were exposed to hydrazine and cured showed no conductivity. The conductivity of the composite films

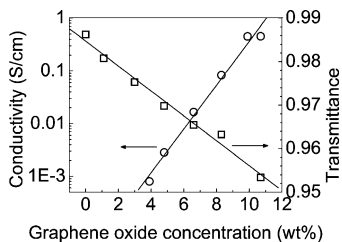


Figure 4. Bulk electrical conductivity (circle) and light transmittance at 650 nm (square) of graphene–silica thin films as a function of the graphene oxide concentration.

changes by almost 3 orders of magnitude, from $(8.0 \pm 0.9) \times 10^{-4}$ S/cm to (0.45 ± 0.06) S/cm, as the loading of graphene oxide increases from 3.9 to 11 wt % (Figure 4). The chemical reduction step appears to be essential for converting insulating graphene oxide sheets into conductive graphene-like sheets and inducing electrical conductivity in composite samples; films that were subjected to curing without chemical reduction were simply nonconductive. Chemical reduction alone renders the uncured hydrazine-treated films sufficiently conductive to be measured with our testing system but only at higher loading levels of the graphene oxide filler ($(1.1 \pm 0.1) \times 10^{-3}$ S/cm at 11 wt % to $(7.0 \pm 0.7) \times 10^{-5}$ S/cm at 9.1 wt %, see Supporting Information). The combination of chemical reduction and high-temperature treatment significantly improved the overall conductivity of the samples. Presumably, the consolidation of the film upon curing (see below) increases the density of the graphene-based sheets inside the matrix, reducing the average intersheet distances (change of film thickness) and resulting in more pathways for electrical conduction.

As expected, incorporation of the graphene oxide sheets into the silica matrix is accompanied by a decrease in the film transparency that is proportional to the weight percentage of the filler. In comparison, the pure silica films behave similarly to glass and are essentially highly transparent over the 380–1000 nm wavelength range (Figure 5a). However, even at the highest loading (11 wt %), the transmittance is consistently high, ranging from 0.94 to 0.96 in the wavelength range of 380–1000 nm. The transparency of the graphene oxide–silica composite is further reduced after chemical reduction and curing (Figure 5b), primarily due to the “graphenization” of the nanofiller, and the transparency at 650 nm drops at most by only 4% after chemical reduction and curing.

Our 11 wt % graphene–silica composite spun-cast films have a bulk conductivity of 0.45 S/cm, comparable to the 0.57 S/cm conductivity reported recently⁴⁸ for a MWCNT/silica sample (with 9.3 wt % CNT loading)⁴⁹ sintered under pressure at elevated temperature. The conductivity of a different MWCNT/silica sample also sintered under pressure and elevated temperature having also 9.3 wt % CNT loading was reported to be $\sim 1 \times 10^{-3}$ S/cm.⁵⁰ It should be noted that our spun-cast films are compared with bulk samples created by high temperature and pressure sintering of sol–gel derived composite. The bulk conductivity of ITO films reported in the literature^{11,12,51} is $\sim 1 \times 10^4$ S/cm. It is significantly higher than that of our 11 wt % graphene–

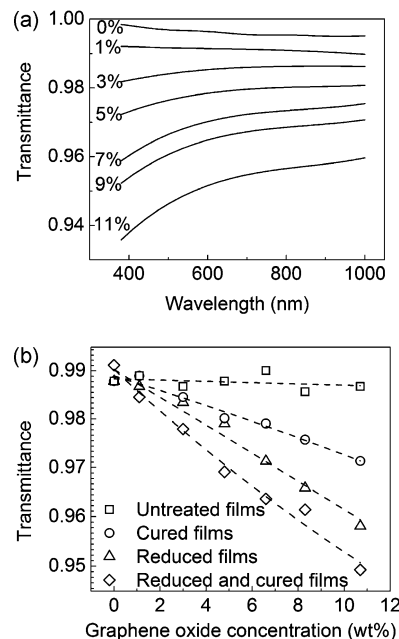


Figure 5. The plots of (a) light transmittance of the hydrazine-reduced and cured composite films vs the wavelength and (b) 650 nm transmittance of composite films that have been subjected to different treatment procedures vs the graphene oxide concentration.

silica composite films; however, our graphene–silica composite films are robust, simple to make, and should not suffer from the problem of long-term ion diffusion commonly encountered with the materials such as ITO.²⁵

In summary, we report the first example of a transparent and electrically conductive ceramic composite of graphene-based sheets. The fabricated films can be made easily via a simple sol–gel route and have excellent potential as a conducting and transparent material. The composite films are very thin and smooth, and the conductive fillers are uniformly distributed throughout the films. The performance of our materials may be improved with higher loading of graphene-based sheets or with chemical modifications of the graphene oxide fillers, details of which will be reported in due course. Not only is our method very effective for incorporation of individual graphene-based sheets into silica matrices, it can potentially be used to modify virtually any hydrophilic surface. In addition to potential applications of our graphene–silica composite as a conducting and transparent material, the ability to coat electrically insulating glass/ceramic substrates with a very thin but conductive layer of this novel material could find many uses as well.

Acknowledgment. We appreciate the support of the NASA University Research, Engineering and Technology Institute on Bio Inspired Materials (BIMat, no. NCC-1-02037), the National Science Foundation (no. CMS-0304506), and the Ministry of Science and Technology, Thailand for a graduate fellowship to SW. SEM and XPS were performed in the EPIC and Keck-II facilities of NUANCE Center at Northwestern University (supported by NSF-NSEC, NSF-MRSEC, Keck Foundation, the State of Illinois, and Northwestern University). We thank the Core Facilities Laboratory in Kaohsiung-Pingtung Area, Taiwan,

for FIB equipment access and technical support. X-ray reflectivity measurements were performed at Beam line X23B of the National Synchrotron Light Source supported by the U.S. Department of Energy. We thank P. B. Messersmith for the use of a UV-vis spectrophotometer and R.-C. Wang for experimental assistance.

Supporting Information Available: Materials and methods, AFM, XRR, and electrical conductivity measurements. This material is available free of charge via the Internet at <http://pubs.acs.org>.

References

- Finley, J. J. *Thin Solid Films* **1999**, *351*, 264–273.
- Romeas, V.; Pichat, P.; Guillard, C.; Chopin, T.; Lehaut, C. *Ind. Eng. Chem. Res.* **1999**, *38*, 3878–3885.
- Smith, J. G., Jr.; Delozier, D. M.; Connell, J. W.; Watson, K. A. *Polymer* **2004**, *45*, 6133–6142.
- Watson, K. A.; Ghose, S.; Delozier, D. M.; Smith, J. G.; Connell, J. W. *Polymer* **2005**, *46*, 2076–2085.
- Beneking, C.; Rech, B.; Wieder, S.; Kluth, O.; Wagner, H.; Frammelsberger, W.; Geyer, R.; Lechner, P.; Rubel, H.; Schade, H. *Thin Solid Films* **1999**, *351*, 241–246.
- Rowell, M. W.; Topinka, M. A.; McGehee, M. D.; Prall, H. J.; Dennler, G.; Sariciftci, N. S.; Hu, L.; Gruner, G. *Appl. Phys. Lett.* **2006**, *88*, 233506-1–3.
- Zhang, J.; Au, K. H.; Zhu, Z. Q.; O'Shea, S. *Opt. Mater.* **2004**, *26*, 47–55.
- Parikh, K.; Cattanaach, K.; Rao, R.; Suh, D. S.; Wu, A.; Manohar, S. K. *Sens. Actuators, B* **2006**, *113*, 55–63.
- Gan, Y.; Liu, J. X.; Zeng, S. N. *Surf. Coat. Technol.* **2006**, *201*, 25–29.
- Wei, Q.; Zheng, H. X.; Huang, Y. H. *Sol. Energy Mater. Sol. Cells* **2001**, *68*, 383–390.
- Betz, U.; Olsson, M. K.; Marthy, J.; Escola, M. F.; Atamny, F. *Surf. Coat. Technol.* **2006**, *200*, 5751–5759.
- Ow-Yang, C. W.; Spinner, D.; Shigesato, Y.; Paine, D. C. *J. Appl. Phys.* **1998**, *83*, 145–154.
- Terzini, E.; Thilakan, P.; Minarini, C. *Mater. Sci. Eng., B* **2000**, *77*, 110–114.
- Chang, J. F.; Wang, H. L.; Hon, M. H. *J. Cryst. Growth* **2000**, *211*, 93–97.
- Camino, D.; Jones, A. H. S.; Mercks, D.; Teer, D. G. *Vacuum* **1999**, *52*, 125–131.
- Konca, E.; Cheng, Y. T.; Weiner, A. M.; Dasch, J. M.; Alpas, A. T. *Surf. Coat. Technol.* **2005**, *200*, 1783–1791.
- Konca, E.; Cheng, Y. T.; Weiner, A. M.; Dasch, J. M.; Alpas, A. T. *Surf. Coat. Technol.* **2006**, *200*, 3996–4005.
- Charitidis, C.; Logothetidis, S. *Thin Solid Films* **2005**, *482*, 120–125.
- Anders, S.; Callahan, D. L.; Pharr, G. M.; Tsui, T. Y.; Bhatnagar, C. S. *Surf. Coat. Technol.* **1997**, *94*–95, 189–194.
- Tong, H. H.; Monteiro, O. R.; Brown, I. G. *Surf. Coat. Technol.* **2001**, *136*, 211–216.
- Maki, K.; Komiya, N.; Suzuki, A. *Thin Solid Films* **2003**, *445*, 224–228.
- Maruyama, T.; Tabata, K. *Jpn. J. Appl. Phys.* **1990**, *29*, L355–L357.
- Rozati, S. M.; Ganj, T. *Renew. Energy* **2004**, *29*, 1671–1676.
- Malaczynski, G. W.; Elmoursi, A. A.; Leung, C. H.; Hamdi, A. H.; Campbell, A. B. *J. Mater. Res.* **2000**, *15*, 590–592.
- Aziz, H.; Popovic, Z. D. *Chem. Mater.* **2004**, *16*, 4522–4532.
- Kim, S. S.; Choi, S. Y.; Park, C. G.; Jin, H. W. *Thin Solid Films* **1999**, *347*, 155–160.
- Ohyama, M.; Kozuka, H.; Yoko, T. *J. Am. Ceram. Soc.* **1998**, *81*, 1622–1632.
- Tsuchiya, T.; Emoto, T.; Sei, T. *J. Non-Cryst. Solids* **1994**, *178*, 327–332.
- Shimono, D.; Tanaka, S.; Torikai, T.; Watari, T.; Murano, M. *J. Ceram. Proc. Res.* **2001**, *2*, 184–188.
- Gong, K. P.; Zhang, M. N.; Yan, Y. M.; Su, L.; Mao, L. Q.; Xiong, S. X.; Chen, Y. *Anal. Chem.* **2004**, *76*, 6500–6505.
- Wei, Y.; Yeh, J. M.; Jin, D. L.; Jia, X. R.; Wang, J. G.; Jang, G. W.; Chen, C. C.; Gumbs, R. W. *Chem. Mater.* **1995**, *7*, 969–974.
- Shimamura, A.; Hubert, Th.; Thust, H. *Surf. Interface Anal.* **2004**, *36*, 1207–1209.
- Gruner, G. *J. Mater. Chem.* **2006**, *16*, 3533–3539.
- Viculis, L. M.; Mack, J. J.; Mayer, O. M.; Hahn, H. T.; Kaner, R. B. *J. Mater. Chem.* **2005**, *15*, 974–978.
- Stankovich, S.; Piner, R. D.; Chen, X.; Wu, N.; Nguyen, S. T.; Ruoff, R. S. *J. Mater. Chem.* **2006**, *16*, 155–158.
- Stankovich, S.; Piner, R. D.; Nguyen, S. T.; Ruoff, R. S. *Carbon* **2006**, *44*, 3342–3347.
- Stankovich, S.; Dikin, D. A.; Dommett, G. H. B.; Kohlhaas, K. M.; Zimney, E. J.; Stach, E. A.; Piner, R. D.; Nguyen, S. T.; Ruoff, R. S. *Nature* **2006**, *442*, 282–286.
- Liu, P.; Gong, K. *Carbon* **1999**, *37*, 706–707.
- Bourlino, A. B.; Gournis, D.; Petridis, D.; Szabo, T.; Szeri, A.; Dekany, I. *Langmuir* **2003**, *19*, 6050–6055.
- Brinker, C. J.; Scherer, G. W. *Sol–Gel Science: The Physics and Chemistry of Sol–Gel Processing*; Academic Press: San Diego, CA, 1990; pp 108–216.
- Hummers, W. S.; Offeman, R. E. *J. Am. Chem. Soc.* **1958**, *80*, 1339–1339.
- All weight percentages are calculated based on the mass of GO and the theoretical mass of silica (SiO₂) produced by the complete hydrolysis of the initial amount of TMOS. It is assumed that this mass ratio is not influenced by the spin-coating step.
- Yu, S.; Wong, T. K. S.; Hu, X.; Goh, T. K. *Thin Solid Films* **2004**, *462*–463, 306–310.
- Almeida, R. M. *Int. J. Optoelectron.* **1994**, *9*, 135–142.
- Bornside, D. E.; Macosko, C. W.; Scriven, L. E. *J. Imaging Sci. Technol.* **1987**, *13*, 122–130.
- Wen, X.; Garland, C. W.; Hwa, T.; Kardar, M.; Kokufuta, E.; Li, Y.; Orkisz, M.; Tanaka, T. *Nature* **1992**, *355*, 426–428.
- Evmenko, G.; van der Boom, M. E.; Kmetko, J.; Dugan, S. W.; Marks, T. J.; Dutta, P. *J. Chem. Phys.* **2001**, *115*, 6722–6727.
- Xiang, C. S.; Pan, Y. B.; Liu, X. J.; Shi, X. M.; Sun, X. W.; Guo, J. K. *J. Nanosci. Nanotechnol.* **2006**, *6*, 3835–3841.
- Xiang, C. S. 2007, private communication.
- Xiang, C. S.; Shi, X. M.; Pan, Y. B.; Guo, J. K. *Key Eng. Mater.* **2005**, *280*–283, 123–126.
- Granqvist, C. G.; Hultaker, A. *Thin Solid Films* **2002**, *411*, 1–5.

NL070477+